

# Pseudospectral versus finite-differences schemes in the numerical integration of stochastic models of surface growth

Rafael Gallego\*

*Departamento de Matemáticas, Universidad de Oviedo, Campus de Viesques, E-33203 Gijón, Spain*

Mario Castro†

*Grupo Interdisciplinar de Sistemas Complejos (GISC) and Grupo de Dinámica No Lineal (DNL),  
Escuela Técnica Superior de Ingeniería (ICAI), Universidad Pontificia Comillas, E-28015 Madrid, Spain*

Juan M. López‡

*Instituto de Física de Cantabria (IFCA), CSIC-UC, E-39005 Santander, Spain*

(Dated: August 2, 2021)

We present a comparison between finite differences schemes and a pseudospectral method applied to the numerical integration of stochastic partial differential equations that model surface growth. We have studied, in 1+1 dimensions, the Kardar, Parisi and Zhang model (KPZ) and the Lai, Das Sarma and Villain model (LDV). The pseudospectral method appears to be the most stable for a given time step for both models. This means that the time up to which we can follow the temporal evolution of a given system is larger for the pseudospectral method. Moreover, for the KPZ model, a pseudospectral scheme gives results closer to the predictions of the continuum model than those obtained through finite difference methods. On the other hand, some numerical instabilities appearing with finite difference methods for the LDV model are absent when a pseudospectral integration is performed. These numerical instabilities give rise to an approximate multiscaling observed in the numerical simulations. With the pseudospectral approach no multiscaling is seen in agreement with the continuum model.

PACS numbers: 81.15.Aa, 05.40.-a, 64.60.Ht, 05.70.Ln

## I. INTRODUCTION

Kinetic surface roughening of surfaces growing in nonequilibrium conditions has been intensively studied for the last two decades [1, 2, 3]. Theoretical approaches make use of both discrete atomistic simulations and stochastic continuum equations for the evolution of the coarse-grained surface height  $h(\mathbf{x}, t)$ . There is overwhelming experimental evidence that surfaces under general nonequilibrium growth conditions can develop scale-invariant correlations in space and time, which supports the hope of a unified theoretical framework to understand kinetic roughening phenomena from first principles. The aim is at identifying the various dynamical universalities of growth associated with different sets of symmetries and/or conservation laws. It is believed that only these basic elements largely determine the universality class and the value of the corresponding critical exponents. In theoretical studies attention is therefore focused on symmetries and only the most relevant terms (in the renormalization group sense) are expected to be required to describe a particular class of growth.

Universality classes of growth are generically represented by stochastic partial differential equations,

$$\partial_t h = \mathcal{G}(\nabla h) + \eta(\mathbf{x}, t), \quad (1)$$

where  $h(\mathbf{x}, t)$  is the height of the interface at substrate position  $\mathbf{x}$  and time  $t$ . The external noise  $\eta(\mathbf{x}, t)$  represents the influx of atoms on the surface. The function  $\mathcal{G}(\nabla h)$  defines a particular model and incorporates the relevant symmetries and conservation laws. In particular, invariance under translation along the growth and substrate directions as well as invariance in the election of the time origin rule out an explicit dependence of  $\mathcal{G}$  on  $h$ ,  $\mathbf{x}$  and  $t$ . Very often the presence of nonlinearities in  $\mathcal{G}$  require the use of perturbative renormalization techniques to obtain analytical approximations for the critical exponents, which can then be compared with Monte Carlo simulations of atomistic models and experiments. A perturbative renormalization approach invariably provides the critical exponents as a series expansion on the parameter  $\epsilon = d_c - d$ , where the critical dimension  $d_c$  can be very high when compared with the dimensions of physical interest (usually  $d = 1$  or  $2$ ). Only in a few lucky cases some extra symmetries produce cancellation of higher order loop diagrams that results in a scaling relation between exponents to be

---

\*rgallego@uniovi.es

†marioc@upcomillas.es

‡lopez@ifca.unican.es

exact to all orders in the perturbative expansion. More often than not, the case is that we only have approximations to the critical exponents valid up to a certain order in  $\epsilon$  and a great deal of elaborated algebraic effort is required to improve our approximation up to the next order. This often makes direct numerical integration of Eq. (1) an extremely useful and necessary tool as the most reliable source of precise values for the critical exponents.

Numerical schemes to integrate continuum surface growth equations like Eq. (1) in  $1 + 1$  and  $2 + 1$  dimensions tend to be unsophisticated. In most cases a straightforward finite-differences (FD) method on a lattice does an excellent job and provides highly precise values for the critical exponents, at least in dimensions of experimental relevance. In this approach (see details below) one basically approximates the continuous height field,  $h(\mathbf{x}, t)$ , by its values on the lattice sites,  $h_i(t)$ , and derivatives by differences between neighboring sites. More clever choices of the discretization rule have been shown to be useful to obtain better agreement with exact properties of the continuum solutions [4], which could not be obtained by using a conventional discretization, like the nominal values of the continuum equation parameters.

However, the use of FD schemes sometimes poses some important problems [5, 6, 7]. In particular Dasgupta *et al.* have shown [8, 9] by means of numerical simulations that discretized versions of commonly studied nonlinear growth equations exhibit an instability in the sense that single pillars (grooves) become unstable when their height (depth) exceeds a critical value. In some cases these instabilities are not present in the corresponding continuum equations, indicating that the behavior of the discretized versions is indeed different from their continuum counterparts. It is important to remark that this pillar/groove instability is actually generic to the FD discretizations of a large class of nonlinear growth equations, including the Kardar-Parisi-Zhang (KPZ) [10] or the Lai-Das Sarma-Villain (LDV) equations [11, 12, 13]. This is a puzzling result because the corresponding continuum equations are *not* unstable.

In many situations, like for instance in KPZ, the existence of this instability is of little significance for practical purposes and one can actually carry out a correct numerical integration by using FD schemes. The reason is that one is mostly interested in the growth from a flat (or almost) surface initial condition and common relaxation mechanisms do not favor the formation of large pillars or grooves. In these cases the instability is only realized if the initial condition is prepared in such a state that there is a pillar/groove of size above the threshold on a otherwise flat surface, which is highly artificial and usually uninteresting for practical purposes. However, as already pointed out in Ref. [9], there is a large class of systems for which the instability of any FD scheme is inevitable. Specifically, discrete versions of models exhibiting anomalous kinetic roughening [14, 15, 16, 17, 18, 19, 20] will certainly show this kind of instability at sufficiently long times. The reason being that anomalous scaling is associated with a nontrivial dynamics of the average surface gradient (local slope), so that  $\langle (\nabla h)^2 \rangle^{1/2} \sim t^\kappa$ , with  $\kappa > 0$  [14, 17]. Therefore, systems exhibiting anomalous roughening will dynamically generate large local height differences, no matter how flat the initial condition is. As a consequence, provided that a simulation is run long enough, the surface will produce pillars/grooves above the critical value for the instability to appear, like for instance is the case for LDV.

One of the models we study in this paper is the LDV equation [11, 12, 13]

$$\partial_t h(\mathbf{x}, t) = -K \nabla^4 h + \lambda \nabla^2 (\nabla h)^2 + \xi(\mathbf{x}, t), \quad (2)$$

where the noise is Gaussian distributed and delta correlated,

$$\langle \xi(\mathbf{x}, t) \xi(\mathbf{x}', t') \rangle = 2D \delta(\mathbf{x} - \mathbf{x}') \delta(t - t'). \quad (3)$$

This model constitutes a minimal model for the long wavelength behavior of surface growth under ideal molecular-beam epitaxy conditions. The LDV model is interesting in many respects and has been the focus of a lot of attention in the literature [11, 12, 13, 17, 20, 21, 22].

Numerical simulations of discrete versions of (2) in  $1 + 1$  dimensions have reported [9] a finite, albeit small, anomalous exponent  $\kappa \approx 0.08$ , possibly indicating a logarithmic dependence. A theoretical prediction [17] based on Flory-type arguments predicted  $\kappa \approx 1/11$  (see however [23]). Therefore, from the discussion above, one would expect a discrete version of (2) to become unstable. This problem was studied by Dasgupta *et al.* and they showed [8, 9] that FD algorithms were actually unstable at long times. They also estimated the critical height step to be around  $h_c(\lambda) \approx A/\lambda$  with  $A \approx 20$  for (2) with  $K = D = 1$ , which clearly shows that the instability will appear the sooner the larger the nonlinear coefficient is. Those authors also found that the addition of higher-order nonlinearities in the FD version of the model controls the numerical instabilities and renders a stable surface, but with intermittent fluctuations and multiscaling properties of surface correlations. It has been claimed that higher-order nonlinearities of the form  $\lambda_{2n} \nabla^2 (\nabla h)^{2n}$ , with  $n > 1$ , may play an important role in LDV universality class because they are infinitely many marginally relevant nonlinear terms [7, 11, 14, 20].

These results can be compared with FD integration schemes for the KPZ equation

$$\partial_t h(\mathbf{x}, t) = \nu \nabla^2 h + \lambda (\nabla h)^2 + \xi(\mathbf{x}, t). \quad (4)$$

It has been shown [8, 9] that discrete versions of Eq. (4) were stable, unless isolated grooves of large enough size are included in the initial state. The reason being that KPZ exhibits conventional (no anomalous) scaling and local slopes are thus rapidly converging towards a constant. Under general conditions the constant is much smaller than the critical slope  $h_c$  for the KPZ discretization to become unstable and so, large slopes are not spontaneously generated by the dynamics.

In reference [29] a study of the 1D and 2D KPZ equation using finite-differences and pseudospectral integration methods is presented. Authors claim that a pseudospectral method gives results closer to the continuum limit than finite-differences methods. They show how a pseudospectral method reproduces the exact value of the global width of the steady state interface within error bars whereas a finite-differences method with conventional discretization of the nonlinear term entails significant differences in the amplitude value. They also use pseudospectral computations to reproduce the most reliable values of the dynamical exponents obtained through discrete growth models.

In this paper we discuss the validity of FD integration algorithms in the presence of anomalous roughening. We compare the accuracy, stability and overall performance of FD methods versus pseudospectral (PS) schemes applied to the paradigmatic examples of the KPZ and LDV equations. We claim that the instability previously found in FD discretizations is spurious and non physical, therefore, FD should be generally avoided in numerical simulations of continuum growth models with anomalous scaling. We argue that the main reason for the adequacy of PS to attack growth problems with anomalous scaling is that spatial derivatives are *more accurate* than in FD methods, where one implicitly assumes that the step height is small. Our conclusions are based on numerical analysis of KPZ and LDV equations in  $1 + 1$  dimensions by means of FD and PS integration schemes. Our results when comparing both techniques are conclusive: (i) PS methods are stable against isolated pillars/grooves, while FD are not, (ii) under the same conditions PS schemes take much longer than FD to get to a numerical overflow, and (iii) PS schemes give well behaved correlation functions with no trace of multiscaling. Finally, we will discuss the implications of our results for the appearance of multiscaling in discrete models proved to be in the same universality class as LDV equations [24].

## II. NUMERICAL INTEGRATION SCHEMES

In order to perform a numerical integration of Eqs. (4) and (2) the parameters can easily be rescaled to have only one independent control parameter—namely, the coupling constant. As it is customary, one can work with dimensionless variables  $h$ ,  $\mathbf{x}$  and  $t$  so that all parameters but one are set to unity, so we have

$$\partial_t h(\mathbf{x}, t) = \nabla^2 h + g(\nabla h)^2 + \eta(\mathbf{x}, t), \quad (5)$$

for the KPZ equation, where the dimensionless coupling constant is  $g = \lambda\sqrt{2D/\nu^3}$ . We can also write the LDV equation in dimensionless form

$$\partial_t h(\mathbf{x}, t) = -\nabla^4 h + g\nabla^2(\nabla h)^2 + \eta(\mathbf{x}, t), \quad (6)$$

where the coupling constant is  $g = \lambda\sqrt{2D/K^3}$  and  $\eta(\mathbf{x}, t)$  is a Gaussian noise with mean zero, unit variance and correlations  $\langle \eta(\mathbf{x}, t)\eta(\mathbf{x}', t') \rangle = \delta(\mathbf{x} - \mathbf{x}')\delta(t - t')$ .

Let us now summarize the idea behind FD and PS integration schemes and introduce some useful definitions. Equations (5) and (6) can be cast in the form

$$\partial_t h(\mathbf{x}, t) = \mathcal{L}[h](\mathbf{x}, t) + \Phi[h](\mathbf{x}, t) + \eta(\mathbf{x}, t), \quad (7)$$

where  $\mathcal{L}[h]$  is a linear functional of  $h$  and  $\Phi[h]$  is another functional containing the nonlinear terms.

### A. Finite-differences methods

We consider a  $d$ -dimensional lattice with periodic boundary conditions with uniform spacing  $\Delta x$  in each direction. The positions of the nodes in the lattice are given by

$$\mathbf{x}_j = \Delta x(j_1, j_2, \dots, j_d), \quad 0 \leq j_i \leq N_i - 1, \quad 1 \leq i \leq d. \quad (8)$$

where  $N_i$  is the lattice size in the  $i$ -th direction. Using a one step Euler's method to compute the temporal derivative, the evolution of a system governed by Eq. (7) is given by:

$$h(\mathbf{x}_j, t + \Delta t) = h(\mathbf{x}_j, t) + \Delta t(\mathcal{L}[h](\mathbf{x}_j, t) + \Phi[h](\mathbf{x}_j, t)) + \sqrt{\frac{\Delta t}{(\Delta x)^d}} \eta(\mathbf{x}_j, t). \quad (9)$$

where  $\Delta t$  is the time step and the stochastic variables  $\eta(\mathbf{x}_j, t)$  have zero mean and correlations  $\langle \eta(\mathbf{x}_j, t)\eta(\mathbf{x}'_j, t') \rangle = \delta_{j,j'}\delta(t - t')$ . We took the  $\eta$  variables as Gaussian random numbers (other distributions can be used as long as they satisfy the central limit theorem).

In finite difference methods, derivatives are computed by truncating the Taylor series of the field up to certain order. Let us introduce the finite difference operators  $\Delta_j^f$  and  $\Delta_j^b$  which are, respectively, the forward and backward difference operators along the  $j$  direction:

$$\Delta_j^f h(\mathbf{x}, t) = h(\mathbf{x} + \mathbf{e}_j \Delta x) - h(\mathbf{x}, t), \quad (10)$$

$$\Delta_j^b h(\mathbf{x}, t) = h(\mathbf{x}, t) - h(\mathbf{x} - \mathbf{e}_j \Delta x). \quad (11)$$

In terms of these operators, the linear parts of Eqs. (5) and (6) are, up to second order of approximation, given by:

$$\mathcal{L}_{\text{KPZ}}(\mathbf{x}_j, t) = (\nabla^2 h)(\mathbf{x}_j, t) = (\Delta x)^{-2} \sum_{i=1}^d \Delta_i^f \Delta_i^b h(\mathbf{x}_j, t),$$

$$\mathcal{L}_{\text{LDV}}(\mathbf{x}_j, t) = -(\nabla^4 h)(\mathbf{x}_j, t) = -\nabla^2(\nabla^2 h) = (\Delta x)^{-4} \sum_{i,j=1}^d \Delta_i^f \Delta_i^b \Delta_j^f \Delta_j^b h(\mathbf{x}_j, t).$$

The explicit expressions in 1 + 1 dimensions are

$$\mathcal{L}_{\text{KPZ}}[h] = (\Delta x)^{-2} (h_{i+1} - 2h_i + h_{i-1}),$$

$$\mathcal{L}_{\text{LDV}}[h] = -(\Delta x)^{-4} (h_{i+2} - 4h_{i+1} + 6h_i - 4h_{i-1} + h_{i-2}),$$

where  $x_i = i\Delta x$ ,  $i = 0, \dots, N-1$  are the positions of the nodes in the lattice and  $h_i = h(x_i, t)$ . Regarding the nonlinear terms we consider for the gradient square the usual symmetric discretization:

$$(\nabla h)^2(\mathbf{x}, t) = \frac{1}{2} (\Delta x)^{-2} \sum_{i=1}^d [(\Delta_i^f + \Delta_i^b)h(\mathbf{x}, t)]^2$$

that in 1 + 1 dimensions becomes

$$(\nabla h)^2(x_i, t) = \frac{1}{2} (\Delta x)^{-2} (h_{i+1} - h_{i-1})^2. \quad (12)$$

In the case of the KPZ equation, other discretizations of the nonlinear term have been proposed [4, 25]. We mention the Lam and Shin discretization (LS) [4]

$$(\nabla h)^2(\mathbf{x}_j, t) = \frac{1}{3} (\Delta x)^{-2} \sum_{i=1}^d \{ [(\Delta_i^f + \Delta_i^b)h(\mathbf{x}_j, t)]^2 - (\Delta_i^f h(\mathbf{x}_j, t)) (\Delta_i^b h(\mathbf{x}_j, t)) \},$$

so that in 1+1 dimensions we have

$$(\nabla h)^2(x_i, t) = \frac{1}{3} (\Delta x)^{-2} [(h_{i+1} - h_i)^2 + (h_{i+1} - h_i)(h_i - h_{i-1}) + (h_i - h_{i-1})^2]. \quad (13)$$

LS discretization has two interesting features in 1+1 dimensions: (i) the effective parameter  $g$  agrees with its nominal value, and (ii) the probability distribution of the discretized version in the steady state can be computed exactly and it turns out to be the probability distribution of the continuum equation for all values of  $g$ . It has been argued [4] that this discretization allows to recover some results predicted by the continuum model while discrepancies when using the conventional discretization (12) have been observed [4].

In the following we use a lattice spacing  $\Delta x = 1$ . As is customary in this kind of simulations, hydrodynamic limit is achieved by increasing the number of lattice sites  $N$ . In numerical integrations of continuous growth models one avoids to perform the  $\Delta x \rightarrow 0$  limit with fixed  $L$ , which would lead the system towards the *linear* critical point, since the coupling constant of the discretized equation is  $g \rightarrow 0$  as  $\Delta x \rightarrow 0$ . A fixed lattice spacing  $\Delta x$  in the limit  $L \rightarrow \infty$  is always preferred as it best drives the system towards the nontrivial critical point.

## B. Pseudospectral method

To compare with FD methods we have considered a numerical scheme consisting of a spectral method in space together with a Euler's method in time. We assume that the field  $h(\mathbf{x}, t)$  satisfies periodic boundary conditions in the multidimensional interval  $[0, L]^d$  and we represent it as a truncated Fourier series

$$h_N(\mathbf{x}, t) = \sum_{\mathbf{k} \in \Gamma_N} \tilde{h}_{\mathbf{k}}(t) e^{i\mathbf{q} \cdot \mathbf{x}}, \quad \mathbf{q} = \frac{2\pi}{L} \mathbf{k}.$$

The set  $\Gamma_N$  over which the sum is taken is given by  $\Gamma_N = \{(k_1, k_2, \dots, k_d) \mid -N/2 \leq k_i \leq N/2 - 1, 1 \leq i \leq d\}$ , and the  $\tilde{h}_{\mathbf{k}}(t)$ 's are the Fourier coefficients of  $h$ , defined as

$$\tilde{h}_{\mathbf{k}}(t) = \frac{1}{L^d} \int_{[0, L]^d} d\mathbf{x} h(\mathbf{x}, t) e^{-i\mathbf{q} \cdot \mathbf{x}}.$$

The noise term  $\eta$  is also replaced by its expansion  $\eta_N$  in Fourier modes. When  $N \rightarrow \infty$  the usual Fourier series is recovered. On the other hand, when  $h$  and  $\eta$  are replaced by  $h_N$  and  $\eta_N$  respectively in Eq. (7), the residual

$$R_N(\mathbf{x}, t) = \partial_t h_N - \mathcal{L}[h_N] - \Phi[h_N] - \eta_N$$

will be not null in general. By requiring  $R_N$  to be orthogonal to the functions  $\{e^{i\mathbf{q} \cdot \mathbf{x}}, \mathbf{k} \in \Gamma_N\}$ , we obtain a set of ODEs for the Fourier coefficients of  $h$ . This procedure is actually equivalent to project the equation onto a subspace of orthogonal polynomials of degree  $\leq N/2$ . Then, by imposing the orthogonality condition

$$\int_{[0, L]^d} d\mathbf{x} R_N(\mathbf{x}, t) e^{-i\mathbf{q} \cdot \mathbf{x}} = 0, \quad \mathbf{k} \in \Gamma_N$$

we obtain

$$\frac{d\tilde{h}_{\mathbf{k}}(t)}{dt} = \omega_{\mathbf{k}} \tilde{h}_{\mathbf{k}}(t) + \tilde{\Phi}_{\mathbf{k}}(t) + \tilde{\eta}_{\mathbf{k}}(t), \quad \mathbf{k} \in \Gamma_N. \quad (14)$$

The quantity  $\omega_{\mathbf{k}}$  is the linear dispersion relation, which is obtained through the Fourier transform of the linear part of the equation; it is  $\omega_{\mathbf{k}} = -\mathbf{q}^2$  for Eq. (5) and  $\omega_{\mathbf{k}} = -\mathbf{q}^4$  for Eq. (6). The  $\tilde{\Phi}_{\mathbf{k}}(t)$ 's are the Fourier coefficients of the nonlinear terms and are given by the following convolution sums:

$$\tilde{\Phi}_{\mathbf{k}}(t) = \begin{cases} -g \sum_{\mathbf{k}_1 + \mathbf{k}_2 = \mathbf{k}} \mathbf{q}_1 \cdot \mathbf{q}_2 \tilde{h}_{\mathbf{k}_1} \tilde{h}_{\mathbf{k}_2} & \text{(KPZ),} \\ g\mathbf{q}^2 \sum_{\mathbf{k}_1 + \mathbf{k}_2 = \mathbf{k}} \mathbf{q}_1 \cdot \mathbf{q}_2 \tilde{h}_{\mathbf{k}_1} \tilde{h}_{\mathbf{k}_2} & \text{(LDV).} \end{cases}$$

Regarding the Fourier coefficients of the noise, it is easy to verify that  $\tilde{\eta}_{\mathbf{k}}(t)$  are complex Gaussian variables with zero mean and correlations

$$\langle \tilde{\eta}_{\mathbf{k}}(t) \tilde{\eta}_{\mathbf{k}'}(t') \rangle = \frac{1}{L^d} \delta_{\mathbf{k}, -\mathbf{k}'} \delta(t - t').$$

The Fourier coefficients  $\tilde{h}_{\mathbf{k}}$  are in general difficult to compute. In addition, even the simplest nonlinearities make it computationally expensive the task of going from real space to Fourier space and viceversa. For these reasons, we consider a discretized space with  $N$  nodes in each direction

$$\mathbf{x}_{\mathbf{j}} = \frac{L}{N} (j_1, j_2, \dots, j_d), \quad 0 \leq j_i \leq N - 1, \quad 1 \leq i \leq d,$$

and we use the discrete Fourier transform  $\mathcal{F}$  to integrate (14). The discrete Fourier coefficients depend only on the values of the field at the nodes  $\mathbf{x}_{\mathbf{j}}$  and are given by (direct discrete Fourier transform):

$$\hat{h}_{\mathbf{k}} = \mathcal{F}[h_{\mathbf{j}}] = \frac{1}{N^d} \sum_{\mathbf{j}} h_{\mathbf{j}}(t) e^{-i\mathbf{q} \cdot \mathbf{x}_{\mathbf{j}}}$$

where  $h_{\mathbf{j}}(t) = h(\mathbf{x}_{\mathbf{j}}, t)$ . We have the inversion formula (inverse discrete Fourier transform):

$$h_{\mathbf{j}}(t) = \mathcal{F}^{-1}[\hat{h}_{\mathbf{k}}] = \sum_{\mathbf{k} \in \Gamma_N} \hat{h}_{\mathbf{k}} e^{i\mathbf{q} \cdot \mathbf{x}_{\mathbf{j}}}.$$

Then, we replace the continuum Fourier coefficients in (14) by the discrete ones, so that

$$\frac{d\hat{h}_{\mathbf{k}}(t)}{dt} = \omega_{\mathbf{k}} \hat{h}_{\mathbf{k}}(t) + \hat{\Phi}_{\mathbf{k}}(t) + \hat{\eta}_{\mathbf{k}}(t). \quad (15)$$

Note that Eq. (15) is now written in terms of the discrete Fourier coefficients  $\hat{h}_{\mathbf{k}}$ . To integrate (15) we perform the following change of variables based on the solution of the linear equation:

$$\hat{h}_{\mathbf{k}}(t) = e^{\omega_{\mathbf{k}}t} \hat{z}_{\mathbf{k}}(t) + \hat{R}_{\mathbf{k}}(t)$$

where

$$\hat{R}_{\mathbf{k}}(t) = e^{\omega_{\mathbf{k}}t} \int_0^t du e^{-\omega_{\mathbf{k}}u} \hat{\eta}_{\mathbf{k}}(u).$$

The  $\hat{z}_{\mathbf{k}}$ 's satisfy the equations

$$\frac{d\hat{z}_{\mathbf{k}}(t)}{dt} = \hat{\Phi}_{\mathbf{k}}(t) e^{-\omega_{\mathbf{k}}t}. \quad (16)$$

The set of ODEs (16) can be solved by using one of the several algorithms available for stochastic differential equations (Euler, Runge-Kutta, predictor-corrector methods, etc.). Considering a one step Euler's method to integrate (16) and going back to the original variable  $\hat{h}_{\mathbf{k}}$ , we are finally left with

$$\hat{h}_{\mathbf{k}}(t + \Delta t) = e^{\omega_{\mathbf{k}}\Delta t} [\hat{h}_{\mathbf{k}}(t) + \Delta t \hat{\Phi}_{\mathbf{k}}(t)] + \hat{r}_{\mathbf{k}}(t). \quad (17)$$

Equation (17) can be reinterpreted as an Euler scheme with time-step (the factor multiplying the nonlinear term)  $e^{\omega_{\mathbf{k}}\Delta t} \Delta t$ , so our algorithm provides a smaller time-step for the smallest length-scales (so it is intrinsically multiscale). This represents a significant improvement with respect to the pseudospectral method used in [29] which is just Eq. (15) integrated with a one step Euler's method.

Assuming that  $\omega_{\mathbf{k}} = \omega_{-\mathbf{k}}$ , the variables  $\hat{r}_{\mathbf{k}}(t)$  can be obtained as

$$\hat{r}_{\mathbf{k}}(t) = \sqrt{\frac{e^{2\omega_{\mathbf{k}}\Delta t} - 1}{2\omega_{\mathbf{k}}}} \frac{1}{(\Delta x)^d} \hat{v}_{\mathbf{k}}(t)$$

where  $\Delta x = L/N$  and  $\hat{v}_{\mathbf{k}}(t)$  are the discrete Fourier transform of a set of Gaussian random numbers of zero mean and unit variance. Note that, as expected, when  $\Delta t \rightarrow 0$  we recover the last term on the right side of Eq. (9).

The computation of the nonlinear terms for the KPZ and LDV equations in Fourier space involves the Fourier transform of the product of two functions (actually, the square of  $\nabla h$ ). In general, calling these two functions  $\sigma$  and  $\rho$ , we need to calculate the convolution sum

$$\hat{\Phi}_{\mathbf{k}} = \sum_{\substack{\mathbf{k}_1 + \mathbf{k}_2 = \mathbf{k} \\ \mathbf{k}_1, \mathbf{k}_2 \in \Gamma_N}} \hat{\sigma}_{\mathbf{k}_1} \hat{\rho}_{\mathbf{k}_2}. \quad (18)$$

In one dimension, this convolution sum implies  $O(N^2)$  operations, which is computationally more expensive than a finite difference method, for which only  $O(N)$  operations are needed. To speed up the computation, we used a *pseudospectral* transform method to compute the Fourier transform of the nonlinear term. Starting from  $\hat{\sigma}_{\mathbf{k}}$  and  $\hat{\rho}_{\mathbf{k}}$ , the inverse transformation is used to obtain  $\sigma$  and  $\rho$  in real space. Then  $\sigma$  and  $\rho$  are multiplied to obtain  $\Phi$  in real space. Finally, the direct Fourier transform is applied to obtain the  $\hat{\Phi}_{\mathbf{k}}$ . In terms of the discrete Fourier operator  $\mathcal{F}$ , this pseudospectral calculation can be written as follows:

$$\hat{\Phi}_{\mathbf{k}} = \mathcal{F}[\mathcal{F}^{-1}[\hat{\sigma}_{\mathbf{k}}] \mathcal{F}^{-1}[\hat{\rho}_{\mathbf{k}}]].$$

This procedure allows to evaluate the convolution sum using  $O(N \log N)$  operations in one dimension. It is important to note that the Fourier coefficients  $\hat{\Phi}_{\mathbf{k}}$  computed in a pseudospectral manner differ from those obtained from a true spectral computation. The difference is the so-called *aliasing error*. For example, in one dimension, the coefficients  $\hat{\Phi}_k$  computed pseudospectrally turn out to be

$$\hat{\Phi}_k = \sum_{k_1 + k_2 = k} \hat{\sigma}_{k_1} \hat{\rho}_{k_2} + \sum_{k_1 + k_2 = k \pm N} \hat{\sigma}_{k_1} \hat{\rho}_{k_2}.$$

The first term on the right hand side is just the convolution sum (18) whereas the second term is the aliasing error. The aliasing error has been proved to be asymptotically of the same order of the error made in truncating the Fourier series. There are several recipes to remove the aliasing. We used a well-known truncation technique usually referred to as the 3/2-rule [27].

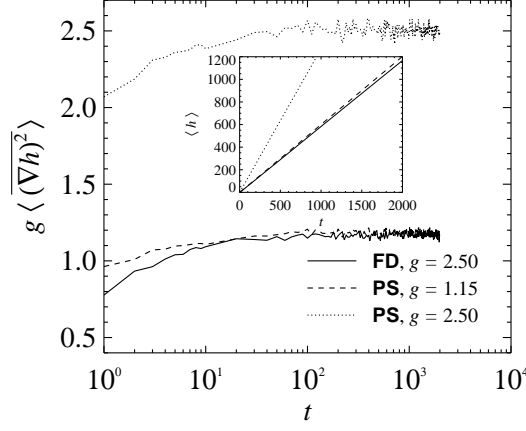


FIG. 1: Average over space and realizations of the nonlinear term for the 1D KPZ equation as a function of time. The inset shows the average height of the interface as a function of time. Here  $L = 128$ , and the averages are taken over 100 realizations. The kind of numerical method and the value of the nonlinear coupling parameter for each curve are shown in the legend.

### III. COMPARISON OF THE METHODS IN 1+1 DIMENSIONS

#### A. Preliminaries

In order to compare the results provided by the FD and PS numerical methods applied to models (5) and (6), we must first notice that, for any given model and the same value of the nonlinear coupling parameter  $g$ , the intensity of the nonlinear effects depends on the numerical scheme used to integrate the equation. This fact, which has already been pointed out in [28], leads to the conclusion that different algorithms cannot in principle be compared directly. In Fig. 1, the average (both over space and realizations) of the nonlinear term for the 1D KPZ equation is shown in several cases. We see that, for the same value of the coupling parameter, the PS method gives effectively a larger nonlinear term. In other words, for the same value of  $g$ , the FD method underestimates the intensity of the nonlinear term with respect to the PS method. A comparison of the two numerical methods can be only made if the nonlinear effects are of the same order for both of them on average.

For the KPZ equation the nonlinear effects can be monitored by measuring the mean velocity of the interface, which is given by

$$v = \frac{g}{L} \int_0^L dx \langle (\nabla h)^2 \rangle.$$

In the inset of Fig. 1 the average height of the interface as a function of time for the 1D KPZ equation is shown. The slope of this curve is just the velocity of the interface. For the same value of  $g$ , the interface obtained with the PS method moves faster. As said before, this indicates that the nonlinear effects are stronger in the PS method than in the FD method. It is easy to find values of  $g$  such that the interface in both cases moves approximately at the same velocity, which means that nonlinear effects are of similar magnitude. Then, if we denote by  $v_{\text{FD}}(g)$  and  $v_{\text{PS}}(g)$  the mean interface velocity for the FD and PS methods, respectively, the value of the coupling parameter  $\tilde{g}$  such that  $v_{\text{PS}}(\tilde{g}) = v_{\text{FD}}(g)$  is given by

$$\tilde{g} = g \frac{v_{\text{FD}}(g)}{v_{\text{PS}}(g)}. \quad (19)$$

The ratio  $v_{\text{FD}}(g)/v_{\text{PS}}(g)$  depends smoothly on both  $g$  and the system size as it can be seen in Fig. 2. The ratio of velocities of the interfaces slightly decreases with  $g$  and increases with the system size. For example, for a system size of  $L = 128$  and  $g = 2.5$ , numerically we have found that  $v_{\text{FD}}(g)/v_{\text{PS}}(g) \approx 0.46$ , which means that the nonlinear effects in the PS method are approximately twice as much stronger than those of the FD method. In Fig. 1 we can see how the nonlinear terms for both integration methods become similar when  $g$  is decreased from 2.5 to a value of  $2.5 \times 0.46 = 1.15$  for the PS method.

In the case of the LDV equation, we can proceed in a similar manner. Let us denote by  $\psi_M(g; t) = g \langle |\nabla^2(\nabla h)^2| \rangle$  the absolute value of the nonlinear term of the LDV equation averaged over space and realizations for the numerical method  $M$ . Then, for a given value of  $g$  used with the FD method, we can estimate a  $\tilde{g}$  for the PS method leading to a nonlinear term of the same order. This is

$$\tilde{g} = g \left\langle \frac{\psi_{\text{FD}}(g; t)}{\psi_{\text{PS}}(g; t)} \right\rangle_t. \quad (20)$$

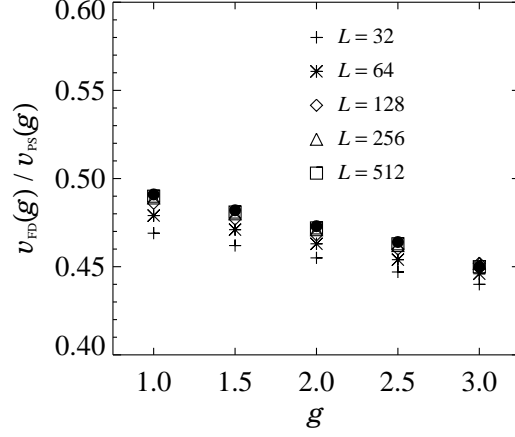


FIG. 2: Ratio  $v_{\text{FD}}/v_{\text{PS}}$  as explained in the text as a function of the nonlinear coupling parameter  $g$  for several system sizes.

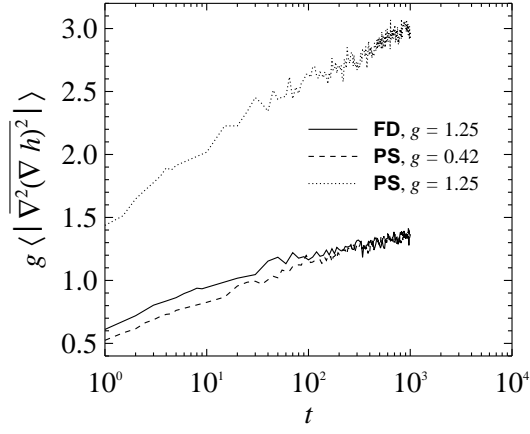


FIG. 3: Average over space and realizations of the absolute value of the nonlinear term for the 1D LDV equation as a function of time. Here  $L = 128$ , and the averages are taken over 100 realizations. The kind of numerical method and the value of the nonlinear coupling parameter for each curve are shown in the legend.

In the previous expression the angular brackets denote an average over the time interval used in the simulation. As for the KPZ equation, the ratio  $\tilde{g}/g$  computed according to Eq. (20) depends slightly on both the system size and  $g$ . For example, for a system size of  $L = 128$  and a value of  $g_{\text{FD}} = 1.25$  used in the FD algorithm, we find that a value of  $g_{\text{PS}} \simeq 0.42$  gives rise to a nonlinear term of the same order for the PS method (see Fig. 3). As occurs for the KPZ equation, the nonlinear effects are stronger for the PS method.

We checked that the global dynamical exponents obtained with the FD and PS methods are the same using values of  $g$  according to (19) and (20). The global interface width scales according to the Family-Vicsek ansatz [30]:

$$W(L, t) = \langle \overline{(h(x, t) - \bar{h})^2} \rangle = t^{\alpha/z} f(L/t^{1/z}),$$

where the scaling function  $f$  behaves as

$$f(u) \sim \begin{cases} u^\alpha & \text{if } u \ll 1, \\ \text{const} & \text{if } u \gg 1. \end{cases}$$

The parameter  $\alpha$  is the roughness exponent,  $z$  is the dynamic exponent, and the ratio  $\beta = \alpha/z$  is the time exponent. In 1+1 dimensions the critical exponents can be computed exactly [10] and their values are  $\alpha = 1/2$  and  $z = 3/2$ , so that  $\beta = 1/3$ . Using the FD with  $g = 2.5$ , we found the exponents  $\alpha \simeq 0.49$ ,  $\beta \simeq 0.32$ ,  $z = \alpha/\beta \simeq 1.52$  for the FD method and with  $g = 1.2$  we obtain the same values of the exponents with the PS method within error bars. For the LDV equation the global exponents are known for arbitrary dimension. In 1+1 dimensions they are  $\alpha = 1$ ,  $\beta = 1/3$ , and  $z = 3$ . Taking a value of  $g = 1.25$  we

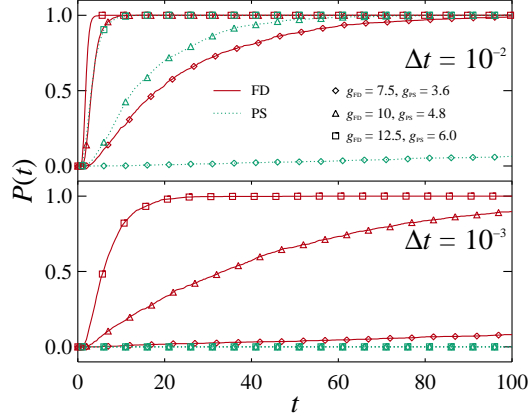


FIG. 4: Probability of instability for the 1D KPZ equation as a function of time. The initial condition is a flat interface. Here  $L = 100$  and the probabilities are computed using 2000 realizations. Curves for two values of the time step are shown. We show results for the FD and PS numerical methods and some different values of the nonlinear coupling parameter  $g$  which are shown in the legend.

found the exact value of the exponents with two significant digits by integrating the equation with the FD method, with system sizes ranging from  $L = 16$  to  $L = 256$  and averaging the interfaces over 100 runs. On the other hand, the PS method with  $g = 0.42$  provides the same exponents within error bars.

### B. Stability of the algorithms

We tested the stability of the algorithms by measuring the probability  $P(t)$  that the system exhibits a numerical overflow when starting from a flat interface. This is measured from a large number of independent runs as the frequency probability of getting a computer overflow at time  $t$ . This numerical instability takes place when the height of the interface tends to grow indefinitely. The probability of instability is a decreasing function of the time step used in the simulations.

In Fig. 4 the probability of instability as a function of time for the 1D KPZ equation is shown for several cases. We show curves for two time steps  $\Delta t = 10^{-2}$  and  $\Delta t = 10^{-3}$ . The system size is  $L = 100$  and the probabilities are computed over 2000 samples. The values of  $g$  were chosen in such a way that the nonlinear effects for the two methods were of the same order. For the KPZ equation this is achieved when  $g_{PS} \simeq 0.48g_{FD}$ . In all cases we found the probabilities for the PS method to be smaller than those of the FD method for a given time step. For example, for a time step of  $\Delta t = 10^{-3}$ , we can see in the bottom graphic of Fig. 4 that the PS method is stable (that is, the probability of instability is equal to zero) in the time interval  $[0, 100]$  for values of  $g = 3.6, 4.8$ , and  $6.0$ , whereas the FD becomes unstable at very short times.

In Fig. 5 we show the probability of instability as a function of time for the 1D LDV equation. In this case we took  $g_{PS} = 0.34g_{FD}$  to match the nonlinear effects for both methods. In much the same way as for the KPZ equation we see that for a given time step the PS method is the most stable. This is also observed for other time steps ranging from  $10^{-5}$  to  $10^{-2}$ . We then conclude that the PS method is the most stable when the intensity of the nonlinear terms are of equivalent magnitude. This means that, under the same conditions, the PS method allows to follow the temporal evolution of the system up to larger times.

### C. KPZ equation

There are some exact results of the continuum KPZ model that we can use to test the numerical methods. First, the steady state probability distribution of the heights is known exactly [1, 2]. In terms of the slopes,  $m(x) = \partial_x h(x)$ , it is known that

$$\mathcal{P}(m) \sim \exp \left[ - \int dx m(x)^2 \right].$$

This expression can be written approximately as:

$$\mathcal{P}(m) \sim \exp \left( - \sum_{i=0}^n \Delta x m_i^2 \right) = \exp \left( - \Delta x m^2 \right).$$

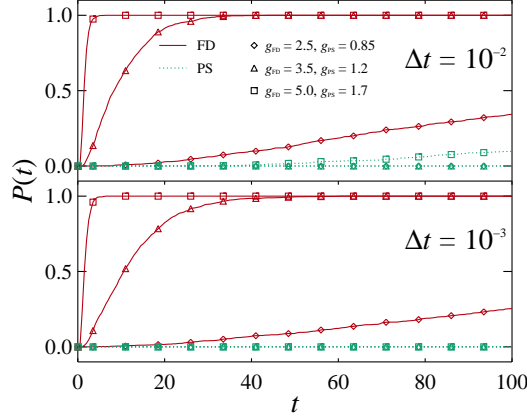


FIG. 5: Probability of instability for the 1D LDV equation as a function of time. The initial condition is a flat interface. Here  $L = 100$  and the probabilities are computed using 2000 realizations. Curves for two values of the time step are shown. We show results for the FD and PS numerical methods and some different values of the nonlinear coupling parameter  $g$  which are shown in the legend.

We have used the central limit theorem to identify  $\sum_{i=0}^n m_i^2$  with  $m^2$ . Here  $m$  represents the slope of the field in the steady state at any point of the lattice. The normalized expression of the probability is:

$$\mathcal{P}(m) = \pi^{-1/2} e^{-m^2}.$$

With this probability distribution, we can find the several moments of the slope  $m$ :  $\langle m^2 \rangle = 1/2$ ,  $\langle m^4 \rangle = 3/4$ ,  $\langle m^6 \rangle = 15/8$ .

For the discretized model and when the LS discretization is used, the steady state distribution probability is found to be [4]

$$P[h_i] \sim \exp \left[ - \sum_{i=0}^N (h_{i+1} - h_i)^2 \right]. \quad (21)$$

It is worth mentioning here a caveat concerning (21). One can see that, in order to reproduce numerically the slope distribution with the FD method, slopes must be computed with the forward (or backward) operator (Eq. (10)), so that  $m_i = h'_i = h_{i+1} - h_i$ . We have checked that if the symmetric rule to compute the derivatives ( $m_i = (h_{i+1} - h_{i-1})/2$ ) is used the width of the slope probability distribution is far from unity, which is the exact value. When forward or backward derivatives are used, however, the correct value is recovered. Remarkably, the PS method provides the proper result in a natural way.

The global interface width in the steady state is also known exactly [21],

$$W(L) = \sqrt{\frac{1}{24}} L^{1/2}, \quad t \rightarrow \infty, \quad (22)$$

and it is independent of the nonlinear coupling parameter  $g$ . In reference [4] it is shown that a FD method with conventional discretization for the nonlinear term, Eq. (12), provides steady state interfaces whose global width is of the form (22) but with a prefactor of  $L^{1/2}$  significantly smaller than the predicted value  $24^{-1/2}$ . It has been argued [4] that with the improved discretization (13) the correct value for the prefactor is recovered. A plot of  $\phi(L) = \sqrt{24/L} W(L)$  versus  $L^{-1}$  was presented in references [26, 29], showing that  $\phi(L)$  is unity within error bars for both the PS method and the FD method with the discretization (13), although the dispersion of the data is larger for the FD method. We have also carried out a similar study comparing FD and PS methods. We checked that the curve  $W(L)$  vs.  $L$  can be fitted to a function of the form  $B L^{1/2}$ , where  $B = 0.182 \pm 0.002$  for the FD method with the usual discretization (12). As expected, this value is clearly smaller than the nominal value  $B_0 = 24^{-1/2} \simeq 0.204$ . This observation is in agreement with that of reference [4]. On the other hand, for both PS and FD method with LS improved discretization (13) we obtain the same value (indistinguishable up to the third digit)  $B = 0.196 \pm 0.003$ , a value very close to  $B_0$  indeed. Therefore, with the PS method we obtain in a natural way the result predicted by the continuum model for the steady state global interface width. For the FD method, on the contrary, we must use an *ad hoc* discretization of the nonlinear terms to achieve the same results.

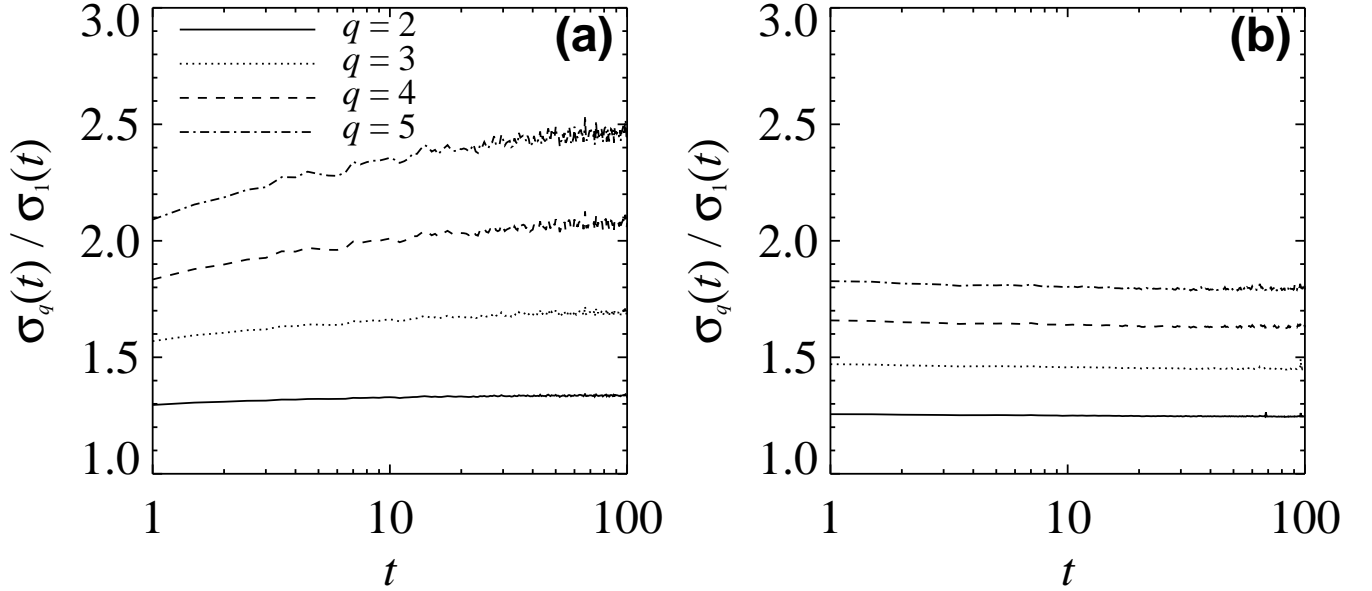


FIG. 6: Ratios  $\sigma_q/\sigma_1$ ,  $q = 2, 3, 4, 5$ , as a function of time, of the moments of the nearest neighbor height difference for the 1D LDV equation integrated with the FD [Fig. (a)] and PS [Fig. (b)] numerical methods. Here  $L = 100$ ,  $g_{FD} = 2$ ,  $g_{PS} = 1.5$ , and the averages are taken over 300 realizations.

#### D. LDV equation

We have investigated the influence of the numerical method on the multiscaling behaviour of the LDV equation. The multiscaling can be detected by looking at the moments of the nearest neighbour height difference. We define [14]

$$\sigma_q(t) = \langle |h_{i+1}(t) - h_i(t)|^q \rangle^{1/q},$$

where the average is taken over each site of the system and over the different realizations of the noise. In systems that exhibit anomalous scaling, as the case of the LDV equation for intermediate times (see note [23]), the moments  $\sigma_q(t)$  are expected to grow as follows

$$\sigma_q(t) \sim t^{\alpha_q/z}, \quad t \ll L^z,$$

where  $L$  is the system size and  $z$  is the dynamical exponent. When the moments scale in a different way, that is, when the  $\alpha_q$ 's depend on  $q$ , the system is said to show multiscaling. As done in [8, 9], we monitorize the multiscaling by looking at the ratios  $\sigma_q(t)/\sigma_1(t)$ ,  $q \geq 2$ . On the other hand, the multiscaling can also be studied by measuring the height difference correlation function [8, 9, 14]. In Fig. 6a we show the ratios  $\sigma_q(t)/\sigma_1(t)$  with  $q = 2, 3, 4, 5$  for the 1D LDV equation integrated with the FD scheme. Parameter values are  $L = 1000$ ,  $g = 2$ , and the averages are taken over 100 realizations. This is in fact a reproduction of Fig. 12 of reference [9]. As can be seen in the picture, the greater the  $q$ , the faster the growth of  $\sigma_q/\sigma_1$  with time. This behaviour implies the existence of multiscaling. For times greater than 100, the evolution of the system cannot be followed due to the presence of numerical instabilities. The authors of [9] claimed that this behavior is related to an instability of the discretized LDV equation against the growth of isolated pillars, which are just height profiles such that the field  $h$  is positive at a certain point while being zero otherwise. For a given a value of the parameter  $g$ , there exists a critical value  $h_c$  of the pillar height beyond which the pillar grows with a certain probability. It is found that this critical height goes as  $h_c \sim g^{-1}$ . On the other hand, the effect of the magnitude of the time step on this instability seems to be very small. For this reason, it is further argued in [9] that this instability is *not* a numerical artifact due to the use of a not small enough integration time step. As we show in the following our results disagree with this interpretation.

Interestingly, we find that the numerical integration of the LDV equation with the PS method has a significant impact on the observed scaling properties. The instability discussed above, which is present with any FD method, is no longer present, at least in the wide range of couplings we studied. Specifically, a pillar like initial condition of the form

$$h_j = \begin{cases} h_0 & \text{if } j = \frac{N-1}{2}, \\ 0 & \text{otherwise.} \end{cases}, \quad \text{with } 0 \leq j \leq N-1, N \text{ odd}, h_0 > 0 \quad (23)$$

never grows with the PS method. In the absence of noise, the temporal derivative of the field (23) is always negative. A straightforward calculation leads to

$$\partial_t h = -\nabla^4 h + g \nabla^2 (\nabla h)^2 = -\frac{h_0 \pi^4}{15L^4} (N^2 - 1)(3N^2 - 7) \approx -\frac{h_0 \pi^4}{5} < 0, \quad L = N \gg 1.$$

Therefore, a pillar of the form (23) always tends to shrink in the deterministic case. Other structures like double pillars, however, might grow in time when their size exceeds a certain value.

In Fig. 6b we show the ratios  $\sigma_q(t)/\sigma_1(t)$ ,  $q = 2, 3, 4, 5$ , for the 1D LDV equation integrated with the PS scheme. In this case we use a value of  $g = 1.5$  for which the nonlinearities are considerably stronger than for the FD method with  $g = 2$ . As it can be observed, the curves do not grow in time, which means that there is no multiscaling. For other values of  $g$  and other system sizes similar results were obtained. It is worth mentioning, however, that the instability does show up when the aliasing is *not* removed. In this case an isolated pillar may grow when its height is larger than a critical value, in much the same way as with the FD method. So, it is strongly recommended to remove aliasing effects when applying a PS method to correctly describe the continuum physics. Note that the aliasing does not actually affect global properties of the system such as multiscaling, the value of the critical exponents, etc. Indeed, we have also carried out a study of the PS method without removing the aliasing because in this case a similar instability of the FD method is present. We have not observed multiscaling in this case either. We then conclude that the multiscaling does not seem to be related to this instability for the PS method.

This analysis leads to the main conclusion of our paper that the existence of multiscaling may depend on the numerical scheme used to integrate the growth model. We argue that the instability (and associated multiscaling behavior) is intrinsic to the numerical integration scheme rather than to the discretization itself, in contrast with the conclusions of Ref. [8, 9]. Our results clearly show that the instability previously found in FD discretizations has to be seen as spurious and inherent to the discretization scheme used. PS integration methods do not show any trace of either instability (when aliasing is properly removed) or multiscaling, representing much more accurately the dynamics and statistics of the continuum problem. We conclude that a PS method should be preferred for surface growth equations with anomalous scaling, because next-neighbor height differences in this case can grow very large.

#### IV. CONCLUSIONS

We have shown that the choice of the numerical method used to integrate certain stochastic models of surface growth may be of paramount importance in the study of some physical properties of the system. We have compared a standard finite difference method with a pseudospectral numerical scheme in the integration of the KPZ and LDV growth models in 1+1 dimensions. As the FD method underestimates the nonlinear effects with respect to the PS method, the nonlinear coupling parameter were tuned up so that the nonlinear terms were of the same order for both numerical methods on average. The global critical exponents, obtained from the global interface width are the same for the two numerical methods.

With regard to the KPZ equation there are some exact results available derived from the continuum model. The expression for the global width of the interface is known in the saturation regime. With the FD method and a standard discretization for the nonlinear term, the amplitude of the width of the numerical interfaces is smaller than that of the continuum. With the spectral approach, on the contrary, numerical results are very close to the predicted value. Nevertheless, it is possible with the finite differences scheme to get close to the continuum model prediction for the width of steady state interfaces, but at the expense of using more sophisticated discretizations.

We have tested the stability of the algorithms by measuring for different time steps the probability of the system to undergo a floating point instability evolving from a flat interface. This instability is related to a numerical overflow in the surface height data. The PS method proved to be the most stable in all the cases we have studied for both models. In the same way, with the PS method it is possible to follow the temporal evolution of the system for longer times than with the FD method.

The LDV equation exhibits anomalous scaling at intermediate times, so that according to [17] (but see also [23]) the average slope of the field is expected to grow in time. Any FD method leads to a numerical instability against the growth of an isolated pillar appears. This instability has been claimed [8, 9] to be the reason why approximate multiscaling is observed in the numerical simulations, although multiscaling is not present in the continuum equation. More importantly, this multiscaling has been interpreted as a real physical effect, which could explain the multiscaling behavior of surface fluctuations observed in atomistic models believed to belong to the LDV universality class. However, our results show that this interpretation is misleading. We have shown that surface multiscaling is not observed with the PS method, regardless of the temporal evolution of isolated pillars. Therefore, surface multiscaling does not seem to be related to this instability for the PS method nor represent any intrinsic physics of the LDV equation as such. In this respect, due to the fact that discrete models can be mapped into continuum equations, in particular the LDV equation [24], our results indicate that multiscaling behavior observed in such systems could be an artifact of the discretization of the dynamics and, consequently, they are not intrinsic to the physical system they are trying to modelize.

### Acknowledgments

This work is supported by the DGI of the Ministerio de Educación y Ciencia (Spain) through Grant Nos. FIS2006-12253-C06-04 and FIS2006-12253-C06-06.

- 
- [1] A. -L. Barabási and H. E. Stanley, *Fractal Concepts in Surface Growth* (Cambridge University Press, Cambridge, 1995).
  - [2] J. Krug, *Adv. Phys.* **46**, 139 (1997).
  - [3] A. Pimpinelli and J. Villain, *Physics of Crystal Growth* (Cambridge University Press, Cambridge, 1998).
  - [4] C. -H. Lam and F. G. Shin, *Phys. Rev. E* **57**, 6506 (1998); *Phys. Rev. E* **58**, 5592 (1998).
  - [5] K. Moser and J. Kertész, *Physica A* **178**, 215 (1991).
  - [6] J. P. Doherty *et. al.*, *Phys. Rev. Lett.* **72** 2041 (1994).
  - [7] Y. Tu, *Phys. Rev. A* **46** R729 (1992).
  - [8] C. Dasgupta, S. Das Sarma, and J. M. Kim, *Phys. Rev. E* **54**, R4552 (1996).
  - [9] C. Dasgupta, J. M. Kim, M. Dutta and S. Das Sarma, *Phys. Rev. E* **55**, 2235 (1997).
  - [10] M. Kardar, G. Parisi, and Y. -C. Zhang, *Phys. Rev. Lett.* **56**, 889 (1986).
  - [11] Z. W. Lai and S. Das Sarma, *Phys. Rev. Lett.* **66**, 2348 (1991).
  - [12] *J. Phys. I (France)* **1**, 19 (1991).
  - [13] D. E. Wolf and J. Villain, *Europhys. Lett.* **13**, 389 (1990).
  - [14] J. Krug, *Phys. Rev. Lett.* **72**, 2903 (1994).
  - [15] S. Das Sarma, S. V. Ghaisas, and J. M. Kim, *Phys. Rev. E* **49**, 122 (1994); S. Das Sarma, *et. al.*, *Phys. Rev. E* **53**, 359 (1996).
  - [16] J. M. López, M. A. Rodríguez, and R. Cuerno, *Phys. Rev. E* **56**, 3993 (1997); *Physica A* **246**, 329 (1997).
  - [17] J. M. López, *Phys. Rev. Lett.* **83**, 4594 (1999).
  - [18] J. J. Ramasco, J. M. López, M. A. Rodríguez, *Phys. Rev. Lett.* **84**, 2199 (2000).
  - [19] J. M. López, M. Castro, and R. Gallego, *Phys. Rev. Lett.* **94**, 166103 (2005).
  - [20] J. K. Bhattacharjee, S. Das Sarma and R. Kotlyar, *Phys. Rev. E* **53**, R1313 (1996).
  - [21] J. Krug, M. Plischke, and M. Siegert, *Phys. Rev. Lett.* **70**, 3271 (1993).
  - [22] J. M. Kim and S. Das Sarma, *Phys. Rev. Lett.* **72**, 2903 (1994).
  - [23] This anomalous exponent should be interpreted as an effective exponent according to recent theoretical results on the necessary conditions for anomalous roughening in local growth models [19]. Nevertheless, the effect at intermediate times (before the truly asymptotic regime referred to in [19]) is to produce a power-law growth of the local slopes and therefore instabilities of the finite-differences integration scheme as described.
  - [24] See for instance C. A. Haselwandter and D. D. Vvedensky, *Phys. Rev. Lett.* **98**, 046102 (2007), and references therein .
  - [25] A. Giacometti and M. Rossi, *Phys. Rev. E* **62**, 1716 (2000).
  - [26] A. Giacometti and M. Rossi, *Phys. Rev. E* **63**, 046102 (2001).
  - [27] C. Canuto, M. Y. Hussaini, A. Quarteroni, and T. A. Zang, *Spectral Methods in Fluid Dynamics*, Springer-Verlag (1998).
  - [28] L. Giada, Ph. D. Thesis, <http://www.mpikg-golm.mpg.de/th/people/lgiada/tesi.ps.gz>
  - [29] L. Giada, A. Giacometti, and M. Rossi, *Phys. Rev. E* **65**, 036134 (2002).
  - [30] F. Family and T. Vicsek, *J. Phys. A* **18**, L75 (1985).
  - [31] J. Krug, P. Meakin, and T. Halpin-Healy, *Phys. Rev. A* **45**, 638 (1992).